SCIENTIFIC REP🞮RTS

Microscopic basis for the band engineering of $Mo_{1-x}W_xS_2$-based heterojunction

Shoji Yoshida[1], Yu Kobayashi[2], Ryuji Sakurada[1], Shohei Mori[2], Yasumitsu Miyata[2,3], Hiroyuki Mogi[1], Tomoki Koyama[1], Osamu Takeuchi[1] & Hidemi Shigekawa[1]

Transition-metal dichalcogenide layered materials, consisting of a transition-metal atomic layer sandwiched by two chalcogen atomic layers, have been attracting considerable attention because of their desirable physical properties for semiconductor devices, and a wide variety of pn junctions, which are essential building blocks for electronic and optoelectronic devices, have been realized using these atomically thin structures. Engineering the electronic/optical properties of semiconductors by using such heterojunctions has been a central concept in semiconductor science and technology. Here, we report the first scanning tunneling microscopy/spectroscopy (STM/STS) study on the electronic structures of a monolayer $WS_2/Mo_{1-x}W_xS_2$ heterojunction that provides a tunable band alignment. The atomically modulated spatial variation in such electronic structures, i.e., a microscopic basis for the band structure of a $WS_2/Mo_{1-x}W_xS_2$ heterojunction, was directly observed. The macroscopic band structure of $Mo_{1-x}W_xS_2$ alloy was well reproduced by the STS spectra averaged over the surface. An electric field of as high as $80 \times 10^6 Vm^{-1}$ was observed at the interface for the alloy with $x = 0.3$, verifying the efficient separation of photoexcited carriers at the interface.

Monolayer transition-metal dichalcogenides (TMDs), consisting of a transition-metal atomic layer (e.g., W and Mo) sandwiched by two chalcogen atomic layers (S, Se and Te), have been attracting considerable attention because of their desirable physical properties for semiconductor devices such as a high optical absorption coefficient[1–3], efficient photoluminescence[4,5], and a valley structure[6–8]. Different combinations of transition metals and chalcogen atoms can provide band gaps varying over a wide range (1–3 eV), and a wide variety of pn junctions, which are essential building blocks for electronic and optoelectronic devices, have been realized using such atomically thin materials[9–15]. The engineering of the electronic/optical properties of semiconductors by using such heterojunctions has been a central concept in semiconductor science and technology, and from a fundamental standpoint, heterostructures formed by two-dimensional materials provide a new platform for exploring new physics.

Recently, tunable band alignment has been realized using $Mo_{1-x}W_xS_2$ alloy[16–19], showing the high potential of this material for future device technology. However, the microscopic view of the electronic structures of $Mo_{1-x}W_xS_2$-based heterojunctions, which is the basis for the band engineering, has not yet been clarified. Here, we report the first scanning tunneling microscopy/spectroscopy (STM/STS) study on the electronic structures of a monolayer $WS_2/Mo_{1-x}W_xS_2$ lateral heterojunction. The atomic-scale analysis by STM/STS allowed the verification of the basic semiconductor physics of this material, providing a microscopic basis for the band engineering.

Results

Atomically modulated electronic structures and macroscopic band structure of $Mo_{1-x}W_xS_2$ alloy.
Monolayer $WS_2/Mo_{1-x}W_xS_2$ lateral heterojunctions for the STM measurements were prepared

[1]Faculty of Pure and Applied Sciences, University of Tsukuba, Tsukuba 305-8573, Japan. [2]Department of Physics, Tokyo Metropolitan University, Hachioji, Tokyo 192-0397, Japan. [3]JST-PRESTO, Kawaguchi, 332-0012, Japan. Correspondence and requests for materials should be addressed to H.S. (email: hidemi@ims.tsukuba.ac.jp)
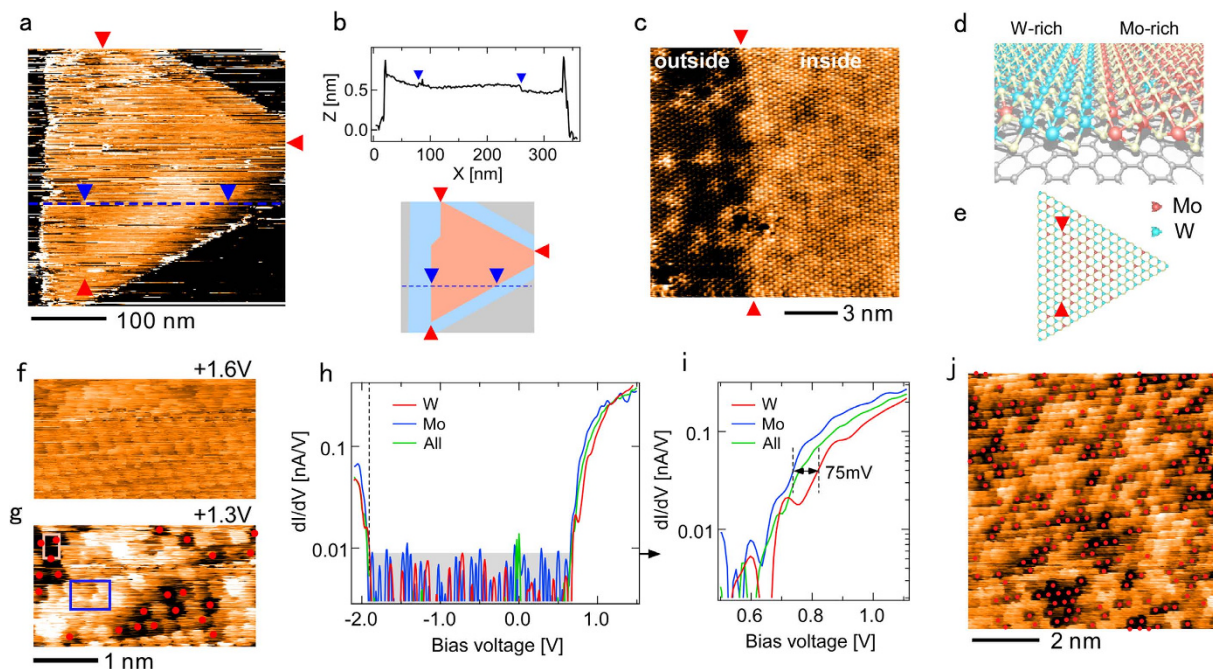
Figure 1. STM/STS on the $WS_2/Mo_{1-x}W_xS_2$ heterostructure. (**a**) STM image of a typical $Mo_{1-x}W_xS_2$ structure grown by CVD on a graphite substrate ($V_s = +2.5$ V, $I_t = 0.25$ A). (**b**) Cross section along the blue line in a and schematic structure of the STM image in (**a**). (**c**) Magnification of the part of the interface indicated by two red triangles at the top and bottom in a. (**d,e**) Schematic models of the STM images in (**c,a**). (**f,g**) STM images of Mo-rich $Mo_{1-x}W_xS_2$ area obtained at sample bias voltages of $V_s = +1.6$ and $+1.3$ V, respectively. (**h**) dI/dV spectra obtained in the Mo and W areas indicated by the white and blue squares in (**g**). The gray rectangle indicates the noise level. (**i**) Magnification of the spectra in (**h**) near the conduction band edge E_{CBM}. (**j**) High-resolution STM image of Mo-rich $Mo_{1-x}W_xS_2$ area.

by chemical vapor deposition (CVD) on a graphite substrate (see Method). All STM/STS measurements were carried out using an Omicron low temperature-STM and a W tip at 87 K.

Figure 1a,b show a typical STM image of $Mo_{1-x}W_xS_2$ monolayer alloy with a triangular shape and the cross section along the blue line in the STM image, respectively. The low resolution of the STM image in Fig. 1a is due to the fact that it was difficult to obtain a high-quality image at a low temperature when the observed area included an island edge. As shown in the cross section, the height of the layer is ~0.7 nm over the triangular structure. Close inspection of Fig. 1a and the cross section reveals a slightly smaller triangular area inside the triangular shape, with the interface between the inner and outer triangles shown by two dark blue triangles. The two triangular structures are schematically shown below the cross section in Fig. 1b, in which the three red triangles indicate the positional relationship with Fig. 1a.

Figure 1c shows a magnification of a part of the interface between the smaller inner triangle and the larger outer triangle along the line joining the two red triangles at the top and bottom of Fig. 1a. The interface in the STM image in Fig. 1c is also indicated by two red triangles. To obtain the Mo and W distributions, the bias voltage was set at $+1.35$ V and the Mo and W atoms were imaged with a suitable contrast. As shown in Fig. 1c, small bright islands are distributed in the outer area (left side of the image), while dark lines form a netlike structure in the inner area (right side of the image), as previously observed for $Mo_{1-x}W_xS_2$ alloy exfoliated from its bulk structure[17]. Namely, the inner triangular area in Fig. 1a (right side of Fig. 1c) is not a second layer but a Mo-rich $Mo_{1-x}W_xS_2$ alloy area surrounded by the W-rich alloy area corresponding to the larger triangle (left side of Fig. 1c), i.e., a heterostructure of W-rich and Mo-rich $Mo_{1-x}W_xS_2$ alloys was successfully formed, as observed for $Mo_{1-x}W_xS_2$ grown on a SiO_2 or sapphire substrate[11–15,18]. Structural models for Fig. 1c,a are schematically shown in Fig. 1d,e, respectively.

The heterojunction interface was formed parallel to the edge of the triangular area. An atomically sharp heterojunction interface is clearly visible in the close-up view of the heterojunction interface shown in Fig. 1c. Such a sharp in-plane compositional variation is considered to be a result of the CVD growth sequence. At the initial growth stage, Mo-rich $Mo_{1-x}W_xS_2$ alloy was formed in the inner triangle by the Mo rich atmosphere around the substrate owing to the high vapor pressure of MoO_3 compared with that of WO_3. Subsequently, the W-rich structure was epitaxially grown from the edge of the Mo-rich structure because of the shortage of Mo and the reduced diffusion of Mo atoms. Similar sequential atomic growth

has been observed in previous studies[11,18]. Although local fluctuation was observed, the compositional distributions of Mo and W atoms, i.e., the ratio between them, were almost the same over the island and among the islands formed in this sample.

Figure 1f,g show the bias dependence of the $Mo_{1-x}W_xS_2$ structure. The STM image is almost flat at a sample bias voltage of $V_s = +1.6$ V, while darker W atoms marked by red circles appeared at $V_s = +1.3$ V, as observed in Fig. 1c. This is in good agreement with the theoretical result that the local density of states near the conduction band edge E_{CBM} is localized at the Mo sites[17]. To observe the electronic structures in more detail, STS measurements were carried out over the W and Mo areas indicated by the white (upper left) and blue squares in Fig. 1g, respectively, and the results are shown in Fig. 1h. Figure 1i shows a magnification of the spectra in Fig. 1h near E_{CBM}. The spectrum denoted by 'All' was obtained by averaging over the surface in Fig. 1g. Although the valence band edges E_{VBM} of the three spectra were located close to each other, E_{CBM} in the Mo area was about 75 meV lower than that in the W area. From the spectrum 'All', the band gap in the area was estimated to be ~2.5 eV, which is between those for pure MoS_2 (2.40 eV)[20] and pure WS_2 (2.73 eV)[21]. Here, E_{CBM} and E_{VBM} were determined using the bias voltages at which the signal became higher than the noise level. The shift of 75 meV was estimated from the shift between the spectra obtained in the Mo and W areas, respectively, at higher bias voltages of 0.7–1.0 V.

In the same manner as in the estimation of composition-dependent photoluminescence (PL) peak energies[16], the band gap E_g of the $Mo_{1-x}W_xS_2$ alloy was estimated using the following equation, where b is the bowing factor;

$$E_g(Mo_{1-x}W_xS_2) = xE_g(WS_2) + (1-x)E_g(MoS_2) - bx(1-x), \qquad (1)$$

Figure 1j shows a high-resolution STM image of the larger Mo-rich area, in which the compositional ratio of W was estimated to be x = 0.3. The bowing factor of b = 0.14 eV given in ref. 16 was employed. Then, E_g ($Mo_{1-x}W_xS_2$) was macroscopically evaluated to be 2.47 eV, which is in good agreement with the experimental value of 2.5 eV obtained by averaging the STS local spectra over the surface.

Localized electronic states of the conduction band. Next, we analyzed the localized electronic states of the conduction band in more detail using the Mo-derived electronic structure. To obtain an area of isolated Mo atoms easily, we carried out CVD growth using a lower Mo content (see Method). Figure 2a shows a high-resolution STM image of isolated Mo atoms in a W-rich $Mo_{1-x}W_xS_2$ area obtained at $V_s = +1.5$ V. Mo atoms are brightly imaged, similarly to in Fig. 1. Figure 2b shows dI/dV spectra obtained above the Mo atom (blue) labeled by A in Fig. 2a and in the WS_2 area (red). Figure 2c shows a magnification of the spectra near E_{CBM}. Since the sample is a monolayer, the measurement is free from tip-induced band bending[22,23]. In the WS_2 area, E_{CBM} was located 0.77 V above the Fermi level E_F and E_{VBM} was located 1.95 eV below E_F. Therefore, the band gap of this $Mo_{1-x}W_xS_2$ monolayer was estimated to be 2.72 eV, which is comparable to that of a pure WS_2 monolayer obtained from a two-photon absorption spectrum (2.73 eV)[21]. Since the compositional ratio of Mo atoms on this surface estimated from the STM image was very low (x = 0.025), the band gap of the WS_2 area of this monolayer is considered to be almost identical to that of the pure WS_2 monolayer. E_{VBM} for the spectrum obtained above the Mo atom was located at an almost identical point to that obtained in the WS_2 area. E_{CBM} for the Mo spectrum is about 50 meV lower than that for the W spectrum.

It is known that the contribution of the metal elements to the valence band electronic state is identical for MoS_2 and WS_2, namely, both are d_{xy} and $d_{x^2-y^2}$ orbitals, while the main contribution of the metal to the conduction band electronic states is the d_{z^2} orbital in MoS_2 but the d_{xy}, $d_{x^2-y^2}$, and d_{z^2} orbitals in WS_2[16,24]. Because of the identical orbital contributions of W and Mo atoms to the valence band, these states are strongly coupled with each other to delocalize the E_{VBM} state, whereas Mo-derived states are localized at E_{CBM} because the contribution of the coupling between the Mo d orbital and the W d orbitals to the conduction band is small. Our experimental results clearly show these characteristics.

To what extent does the Mo-derived localized electronic state affect the neighboring WS_2 area? Figure 2d shows an STM image of the area shown in Fig. 2a obtained at $V_s = +1.2$ V to highlight the Mo-derived electronic state. As expected, some W atoms near the Mo atoms are imaged brighter than those in the WS_2 area. To show this effect more clearly, the variation in E_{CBM} near the Mo atoms labeled A, B, and C in Fig. 2d is mapped in Fig. 2e. The value at each of the 75×75 pixel was derived from the onset bias voltage ($dI/dV_{onset} = 0.01$ nA/V) of each dI/dV spectrum. Figure 2f shows the cross section along the dashed line in Fig. 2e. A gradual decrease in E_{CBM} toward the Mo atom can be observed in Fig. 2f. The variation in E_{CBM} around Mo atoms A, B and C are indicated by dotted circles (1.5 nm diameter) in Fig. 2e. This is the first demonstration of the atomically resolved spatial variation in the localized electronic structure of Mo in $Mo_{1-x}W_xS_2$ alloy.

Spatial variation in the band structure of WS_2/$Mo_{1-x}W_xS_2$ heterojunction. Finally, the band structure of the heterojunction interface was analyzed. Figure 3a shows an STM image of a $Mo_{1-x}W_xS_2$-based heterojunction interface similar to that in Fig. 1c, where the left and right regions correspond to W- and Mo-rich $Mo_{1-x}W_xS_2$ monolayers, respectively. To investigate the inner potential of the heterojunction, STS was carried out over the surface. The inset in Fig. 3a shows the STM image simultaneously obtained with the STS measurement.
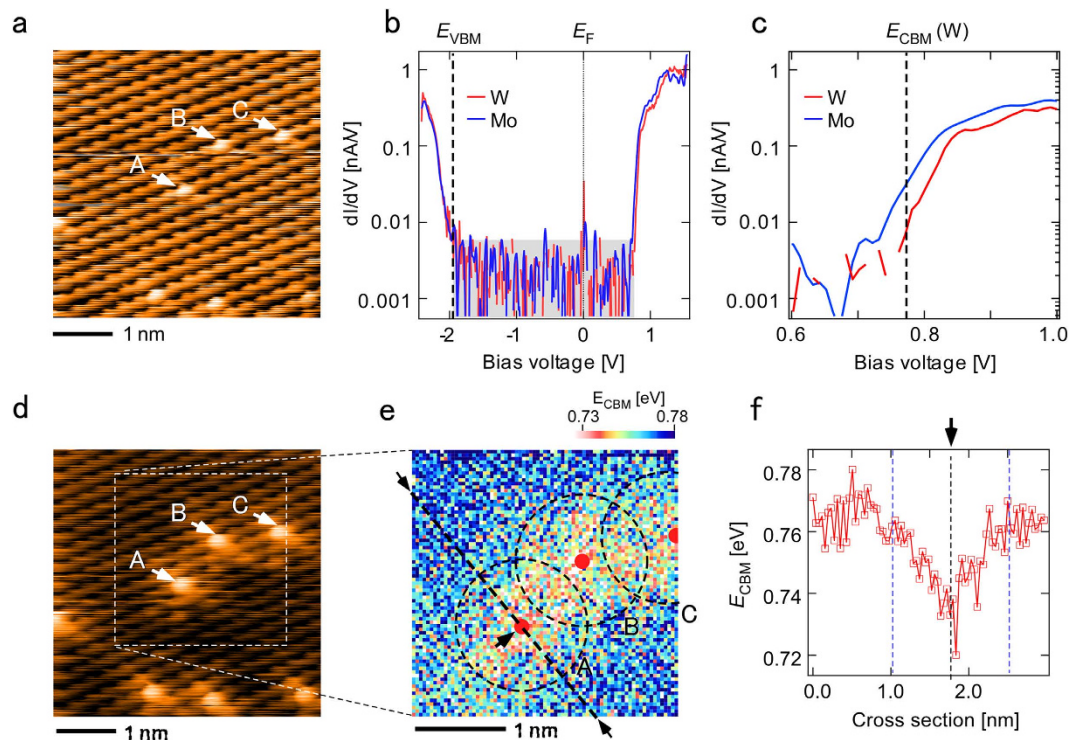
Figure 2. STM/STS on single Mo atoms. (a) STM image of an area with isolated single Mo atoms in a WS_2 area ($V_s = +1.5\,V$, $I_t = 0.1\,nA$). **(b)** dI/dV spectra obtained above Mo atom labeled A in (**a**) and in WS_2 area. The gray rectangle indicates the noise level. **(c)** Magnification of the spectra in b near E_{CBM}. **(d)** STM image of the area shown in a obtained at $V_s = +1.2\,V$. **(e)** Map of the variation in E_{CBM} near the Mo atoms A, B, and C in (**d**). **(f)** Cross section along the dashed line in (**e**). The circles in e indicate the area of influence of the Mo-derived state determined from the cross section in (**f**). The red dots in e indicate the positions of Mo atoms.

Figure 3b shows a map of color scale dI/dV curves calculated from the spatially resolved STS spectra measured along the white dashed line in the inset of Fig. 3a. The upper and lower edges of the band gap region, corresponding respectively to E_{CBM} and E_{VBM}, continuously shifted as a function of the distance across the interface, whose position was determined from the STM image (Fig. 3a inset) and is indicated by the dashed black line in Fig. 3b. Figure 3b clearly demonstrates that a type-II staggered gap heterojunction with a nanoscale built-in potential distribution was formed at the interface[9,14,25,26]. This is the first observation of the electronic structure of a TMD heterojunction. The spatial variation of E_{CBM} over the surface in Fig. 3a was mapped in Fig. 3c to visualize the electrostatic potential landscape at the interface in more detail, which is almost flat along the direction of the interface compared with the change along the direction crossing the interface (from pink to dark blue).

To better understand the positional relationship between the interface and the electrostatic potential variation, the cross section profile of the E_{CBM} map along the dashed line in Fig. 3c (white dotted line in Fig. 3a inset) was plotted (Fig. 3d top) along with the profile of E_{VBM} (Fig. 3d middle) along the line at the same position. The comparison of the topographic image with the cross sections of E_{CBM} and E_{VBM} reveals that the variation in the potential was greater on the Mo-rich side. Namely, E_{CBM} is almost constant in the W-rich area, while it gradually changes over the Mo-rich area, possibly reflecting the asymmetric carrier screening length, which may be due to the difference in the doping characteristics and/or dielectric constant between the W-rich and Mo-rich areas. In addition, the profile of the electric field E_{field} was obtained from the derivative of the E_{CBM} profile with respect to the lateral distance (Fig. 3d bottom). As expected from classical semiconductor theory, the electric field reached its maximum value at the interface position indicated by the dashed line in Fig. 3b,d. The strong electric field of as high as $80 \times 10^6\,Vm^{-1}$ observed at the interface is consistent with the observed charge separation efficiency at the interface[11].

The red and blue spectra shown in Fig. 3e are the dI/dV spectra obtained at the positions indicated by red and blue arrows in Fig. 3b, respectively, where neither E_{CBM} nor E_{VBM} is affected by the built-in potential at the interface. The spectra were averaged over the left and right edges of the inset of Fig. 3c, respectively. From these spectra, the band offsets of E_{CBM} and E_{VBM} between the W-rich and Mo-rich areas were determined to be 0.30 eV and 0.17 eV, and the band gaps of these areas were also determined
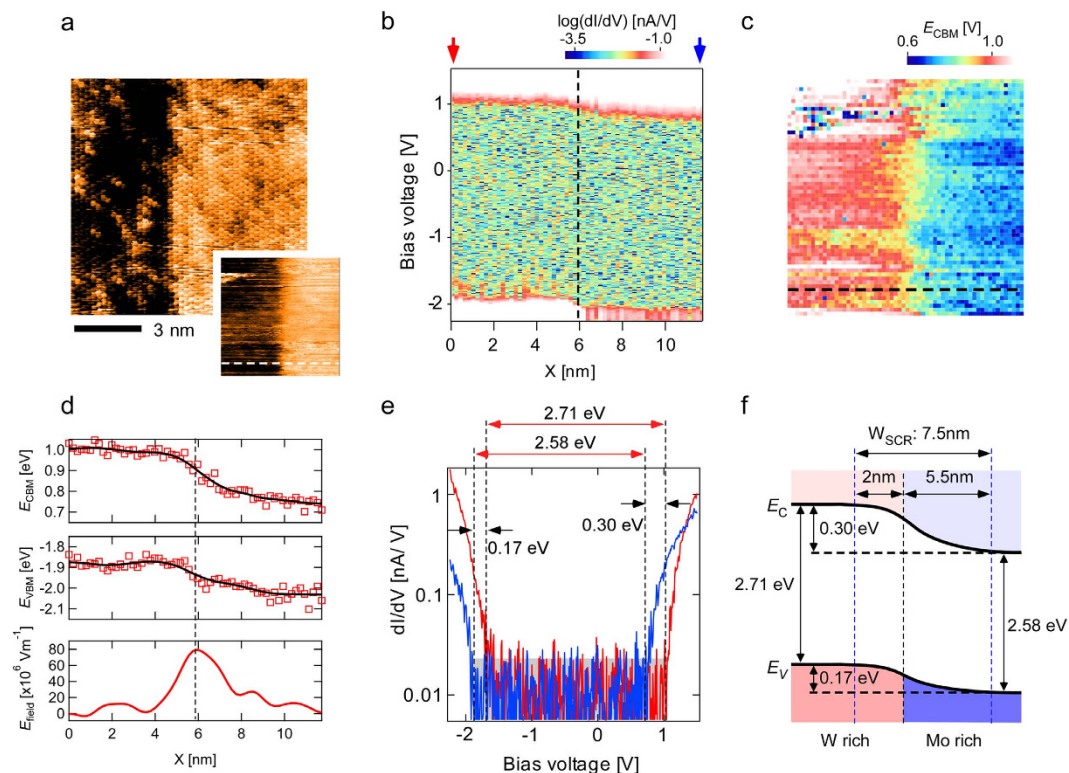
Figure 3. Potential landscape of $WS_2/Mo_{1-x}W_xS_2$ interface. (**a**) STM image of $WS_2/Mo_xW_{1-x}S_2$ interface ($V_s = +1.6\,V$, $I_t = 0.3\,nA$). The inset shows the STM image simultaneously obtained with spectroscopy. (**b**) Map of color scale dI/dV curves calculated from the spatially resolved STS spectra measured along the white dashed line in the inset of (**a**). (**c**) Map of E_{CBM} obtained over the area shown in (**a**). (**d**) Cross sections of E_{CBM} (top) and E_{VBM} (middle), respectively corresponding to the upper and lower edges in (**b**), and electric field E_{field} (bottom) obtained by differentiating the cross section of E_{CBM} (top). (**e**) dI/dV spectra obtained at the positions indicated by red and blue arrows in (**b**), which were averaged over the left and right edge lines in the inset of (**a**), respectively. The gray rectangle indicates the noise level. (**f**) Schematic image of the band structure of the $WS_2/Mo_{1-x}W_xS_2$ heterojunction. The values in (**f**) are those in (**e**). W_{SCR} indicates the width of space charge region.

to be 2.71 eV and 2.58 eV, respectively. Figure 3f shows the first ever schematic image of the band profile of a $WS_2/Mo_{1-x}W_xS_x$ obtained from the experimental results.

In conclusion, we carried out atomically resolved analysis by low-temperature STM/STS on the electronic structures of a monolayer $WS_2/Mo_{1-x}W_xS_2$ alloy heterojunction that provides a tunable band alignment. The formation of a $WS_2/Mo_{1-x}W_xS_2$ heterojunction on a graphite substrate was confirmed for the first time. Then the atomically modulated spatial variation in the electronic structures, which is the basis for the macroscopic band structure of the $WS_2/Mo_{1-x}W_xS_2$ heterojunction, was directly observed. The macroscopic band structure of $Mo_{1-x}W_xS_2$ alloy was reproduced by the STS spectra averaged over the surface. An electric field of as high as $80 \times 10^6\,Vm^{-1}$ was observed at the interface for the alloy with x = 0.3, verifying the efficient separation of photoexcited carriers at the interface. The atomic-scale analysis of TMD heterostructures by STM/STS allows the verification of basic semiconductor physics and is expected to play an essential role in the further advancement of various applications.

Method

Sample preparation. Monolayer $WS_2/Mo_{1-x}W_xS_2$ lateral heterojunctions were formed on Kish graphite (Covalent Materials Co.) by high-temperature chemical vapor deposition[28]. The graphite was mechanically exfoliated onto a quartz substrate using Nitto tape (SPV-224). The substrate was placed in a quartz tube (3 cm diameter, 100 cm long) with WO_3 powder (Aldrich, 99% purity, 100 mg), MoO_3 powder (Aldrich, 99% purity, 0.2 mg, reduced to 0.1 mg for the measurement of the effect of a single Mo atom shown in Fig. 2), and sulfur flakes (Aldrich, 99.99% purity, 2 g). The quartz tube was then filled with Ar gas at a flow rate of 100 cm³/min. The temperature of the substrate and the WO_3 and MoO_3 was gradually increased to the growth temperature (1100 °C) over 60 min using an electrical furnace. When the substrate temperature reached the set value, the sulfur was heated at 200 °C for 15–30 min to supply sulfur vapor to the substrate using another electrical furnace. After the growth, the quartz tube was immediately cooled using an electric fan.

References

1. Bernardi, M., Palummo, M. & Grossman, J. C. Extraordinary sunlight absorption and one nanometer thick photovoltaics using two-dimensional monolayer materials. *Nano Lett.* **13**, 3664–3670 (2013).
2. Yu, Y. *et al.* Equally Efficient Interlayer Exciton Relaxation and Improved Absorption in Epitaxial and Nonepitaxial MoS$_2$/WS$_2$ Heterostructures. *Nano Lett.* **15**, 486–491 (2014).
3. Kozawa, D. *et al.* Photocarrier relaxation pathway in two-dimensional semiconducting transition metal dichalcogenides. *Nat. Commun.* **5**, 4543 (2014).
4. Splendiani, A. *et al.* Emerging photoluminescence in monolayer MoS$_2$. *Nano Lett.* **10**, 1271–1275 (2010).
5. Mak, K. F., Lee, C., Hone, J., Shan, J. & Heinz, T. F. Atomically thin MoS$_2$: A new direct-gap semiconductor. *Phys. Rev. Lett.* **105**, 136805 (2010).
6. Xu, X., Yao, W., Xiao, D. & Heinz, T. F. Spin and pseudospins in layered transition metal dichalcogenides. *Nat. Phys.* **10**, 343–350 (2014).
7. Mak, K. F., McGill, K. L., Park, J. & McEuen, P. L. Valleytronics. The valley Hall effect in MoS$_2$ transistors. *Science* **344**, 1489–1492 (2014).
8. Zhang, Y. J., Oka, T., Suzuki, R., Ye, J. T. & Iwasa, Y. Electrically Switchable Chiral Light- Emitting Transistor. *Science* **344**, 725–728 (2014).
9. Kang, J., Tongay, S., Zhou, J., Li, J. & Wu, J. Band offsets and heterostructures of two-dimensional semiconductors. *Appl. Phys. Lett.* **102**, 012111 (2013).
10. Xia, F., Wang, H., Xiao, D., Dubey, M. & Ramasubramaniam, A. Two-dimensional material nanophotonics. *Nat Phot.* **8**, 899–907 (2014).
11. Gong, Y. *et al.* Vertical and in-plane heterostructures from WS$_2$/MoS$_2$ monolayers. *Nat. Mater.* **13**, 1135–1142 (2014).
12. Duan, X. X. *et al.* Lateral epitaxial growth of two-dimensional layered semiconductor heterojunctions. *Nat. Nanotechnol.* **9**, 1024–1030 (2014).
13. Zhang, X., Lin, C., Tseng, Y., Huang, K. & Lee, Y. Synthesis of lateral heterostructures of semiconducting atomic layers. *Nano Lett.* **15**, 410–415 (2015).
14. Lee, C.-H. *et al.* Atomically thin p-n junctions with van der Waals heterointerfaces. *Nat. Nanotechnol.* **9**, 676–681 (2014).
15. Huang, C. *et al.* Lateral heterojunctions within monolayer semiconductors. *Nat. Mater.* **13**, 1096–1101 (2014).
16. Chen, Y. *et al.* Tunable band gap photoluminescence from atomically thin transition-metal dichalcogenide alloys. *ACS Nano* **7**, 4610–4616 (2013).
17. Dumcenco, D. O., Kobayashi, H., Liu, Z., Huang, Y.-S. & Suenaga, K. Visualization and quantification of transition metal atomic mixing in Mo$_{1-x}$W$_x$S$_2$ single layers. *Nat. Commun.* **4**, 1351 (2013).
18. Zheng, S. *et al.* Monolayers of Mo$_{1-x}$W$_x$S$_2$ alloy heterostructure with in-plane composition variations. *Appl. Phys. Lett.* **106**, 063113 (2015).
19. Kobayashi, Y., Mori, S., Maniwa, Y. & Miyata, Y. Bandgap-tunable lateral and vertical heterostructures based on monolayer Mo$_{1-x}$W$_x$S$_2$ alloys. *Nano Res.* doi: 10.1007/s12274-015-0826-7 (2015).
20. Huang, Y. L. *et al.* Bandgap tunability at single-layer molybdenum disulphide grain boundaries. *Nat. Commun.* **6**, 6298 (2015).
21. Zhu, B., Chen, X. & Cui, X. Exciton Binding Energy of Monolayer WS$_2$. *Sci. Rep.* **5**, 9218 (2014).
22. Yoshida, S. *et al.* Microscopic basis for the mechanism of carrier dynamics in an operating p-n junction examined by using light-modulated scanning tunneling spectroscopy. *Phys. Rev. Lett.* **98**, 026802 (2007).
23. Ugeda, M. M. *et al.* Observation of giant bandgap renormalization and excitonic effects in a monolayer transition metal dichalcogenide semiconductor. *Nat. Mater.* **13**, 1091–1095 (2014).
24. Tongay, S. *et al.* Two-dimensional semiconductor alloys: Monolayer Mo$_{1-x}$W$_x$Se$_2$. *Appl. Phys. Lett.* **104**, 012101 (2014).
25. Liang, Y., Huang, S., Soklaski, R. & Yang, L. Quasiparticle band-edge energy and band offsets of monolayer of molybdenum and tungsten chalcogenides. *Appl. Phys. Lett.* **103**, 042106 (2013).
26. Koåmider, K. & Fernández-Rossier, J. Electronic properties of the MoS$_2$-WS$_2$ heterojunction. *Phys. Rev. B - Condens. Matter Mater. Phys.* **87**, 075451 (2013).
27. Hong, X. *et al.* Ultrafast charge transfer in atomically thin MoS$_2$/WS$_2$ heterostructures. *Nat. Nanotechnol.* **9**, 682–686 (2014).
28. Kobayashi, Y. *et al.* Growth and Optical Properties of High-Quality Monolayer WS$_2$ on Graphite. *ACS Nano* **9**, 4056–4063 (2015).

Acknowledgements

Author Contributions

S.Y. carried out the experiments with R.S., H.M. and T.K. Mo$_{1-x}$W$_x$S$_2$/graphite samples were prepared by Y.M., S.M., Y.K. and O.T. provided technical assistance. H.S. supervised the project, analyzed the data with S.Y. and edited the paper with S.Y. and Y.M.

Additional Information

Competing financial interests: The authors declare no competing financial interests.

How to cite this article: Yoshida, S. *et al.* Microscopic basis for the band engineering of Mo$_{1-x}$W$_x$S$_2$-based heterojunction. *Sci. Rep.* **5**, 14808; doi: 10.1038/srep14808 (2015).